Geochemistry Geophysics Geosystems G3

Article
Volume 14, Number 1
31 January 2013
doi:10.1029/2012GC004276
ISSN: 1525-2027

Published by AGU and the Geochemical Society

Correlation of ignimbrites using characteristic remanent magnetization and anisotropy of magnetic susceptibility, Central Andes, Bolivia

Michael H. Ort
SESES, Box 4099, Northern Arizona University, Flagstaff, Arizona, 86011, USA (michael.ort@nau.edu)

Shanaka L. de Silva
CEOAS, Oregon State University, Corvallis, Oregon, USA

Néstor Jiménez C.
Instituto de Investigaciones Geológicas y del Medio Ambiente, Universidad Mayor de San Andrés, La Paz, Bolivia

Brian R. Jicha and Bradley S. Singer
Department of Geoscience, University of Wisconsin–Madison, Madison, Wisconsin, USA

[1] Large ignimbrite flare-ups provide records of profound crustal modification during batholith formation at depth. The locations of source calderas and volumes and ages of the eruptions must be determined to develop models for the tectonomagmatic processes that occur during these events. Although high-precision isotopic ages of the ignimbrites are critical, less expensive and more rapid techniques, such as paleomagnetism, can extend the temporal information from dated outcrops. Paleomagnetic and rock magnetic data, including characteristic remanent magnetization (ChRM) and anisotropy of magnetic susceptibility (AMS), from the Altiplano-Puna Volcanic Complex of the Central Andes reliably identify calderas and eight associated Mio-Pliocene ignimbrites.

[2] ChRM results indicate a larger between-site error for most ignimbrites, in comparison to within-site scatter. Part of this dispersion may be due to tumescence/detumescence associated with the caldera-forming eruptions, but most of the effect is probably due to the recording of paleosecular variation during cooling and vapor-phase crystallization of the thick ignimbrites. AMS data identify the source calderas for four ignimbrites and provide limits on possible post-emplacement rotations of the deposits. AMS data indicate significant topographic control on inferred flow directions, implying that the flows were dense and/or of low mobility.

Components: 10,800 words, 9 figures, 3 tables.

Keywords: Altiplano-Puna Volcanic Complex; Ignimbrite correlation; Paleomagnetism; Anisotropy of magnetic susceptibility.

Index Terms: 1518 Computational Geophysics: Magnetic Fabrics and Anisotropy; 1520 Computational Geophysics: Magnetostratigraphy; 8440 Volcanology: Caldera; 8414 Volcanology: Eruption Mechanisms and Flow Emplacement; 8428 Volcanology: Explosive Volcanism.

Received 5 June 2012; **Revised** 9 November 2012; **Accepted** 13 November 2012; **Published** 31 January 2013.

Ort, M. H., S. L. de Silva, N. Jiménez C., B. R. Jicha, and B. S. Singer (2013), Correlation of ignimbrites using characteristic remanent magnetization and anisotropy of magnetic susceptibility, Central Andes, Bolivia, *Geochem. Geophys. Geosyst.*, *14*, 141–157, doi:10.1029/2012GC004276.

1. Introduction

[3] Fueled by elevated thermal flux from the mantle, large 'ignimbrite flare-ups' are regional in scale (>100,000 km^2) and long-lived (several to tens of millions of years) surface manifestations of profound crustal modification [*Elston*, 1984; *Best and Christiansen*, 1991; *de Silva et al.*, 2006; *Lipman*, 2007]. They are characterized by multi-cyclic caldera complexes that erupt hundreds to thousands of cubic kilometers of calc-alkaline dacitic to rhyolitic ignimbrites in each eruption, along with abundant effusive volcanism. Ignimbrites provide nearly instantaneous samples of the magmatic systems in the developing batholith beneath the region [*Smith*, 1979; *Hildreth*, 1981; *Lipman*, 1984] and thus can provide information on the tectonomagmatic processes associated with crustal modification [*Bachmann et al.*, 2007]. Understanding such broader processes requires a complete geologic, stratigraphic and geochronologic framework that identifies source calderas, reveals the full extents of the ignimbrites, and allows accurate estimates of volumes and dates of eruptions. This is achieved through geologic mapping coupled with correlation of the widespread and commonly isolated ignimbrite exposures using multiple methods [*Hildreth and Mahood*, 1985; *de Silva and Francis*, 1989]. Paleomagnetic data are effective correlation tools and, when combined with geochronologic information, can provide a complete spatiotemporal framework for an ignimbrite flare-up.

[4] The Altiplano-Puna Volcanic Complex (APVC) in the Central Andes (Figure 1) is the result of one of the youngest ignimbrite flare-ups on Earth. A recent campaign of high-precision $^{40}Ar/^{39}Ar$ geochronology shows that the large-volume ignimbrites range in age from late Miocene to Pliocene [*Salisbury et al.*, 2011]. Activity has waned since about 4 Ma, and no major ignimbrite eruptions have occurred since ca. 0.7 Ma, although effusive eruptions as young as 89 ka are related to the APVC [*Watts et al.*, 1999]. Geophysical evidence shows a large low-velocity zone (the Altiplano-Puna Magma Body) underlies the region [*Zandt et al.*, 2003] and recent rapid uplift [*Pritchard and Simons*, 2002] and active geothermal areas imply that future activity is still possible.

[5] The geologic features of the APVC are very well exposed due to the arid nature of the Altiplano-Puna

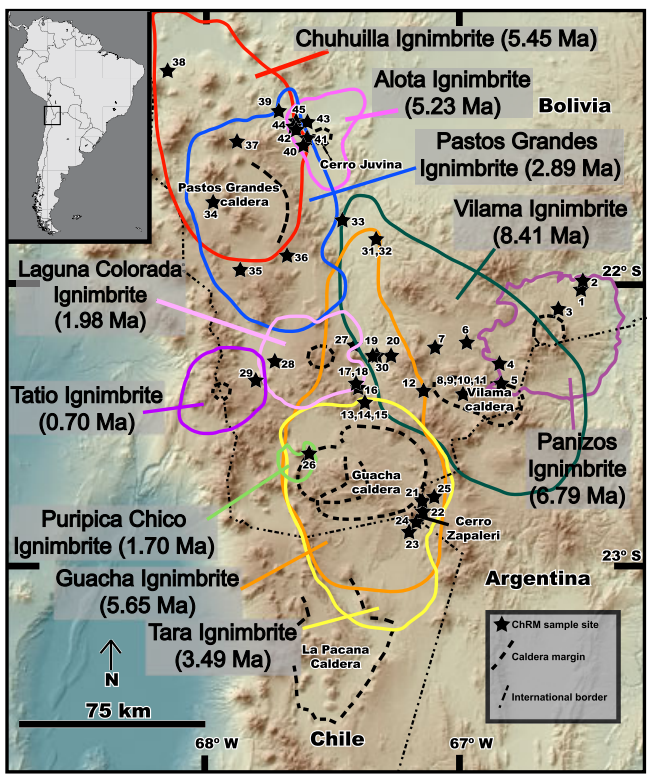

Figure 1. Map of the Altiplano-Puna volcanic complex, showing the distribution of the ignimbrites and sample sites for this study. Extent of known outcrop for each ignimbrite is shown, along with their ages [from *Salisbury et al.*, 2011]. Sample sites are shown as stars with numbers. Colored lines correspond to outcrop extent of each ignimbrite. Inset map shows the location within South America.

region. Large calderas that may not be visible from the ground can be more clearly defined using satellite imagery [*de Silva and Francis*, 1991]. Some ignimbrites with broad distribution have not previously been linked to their source calderas, and the ignimbrites at many outcrops are of unknown origin. The areal extents of the APVC ignimbrites overlap and, because they are macroscopically very similar, it can be difficult to determine which ignimbrite is present at a given outcrop. This makes it difficult to estimate their total volume and, hence, magma production rates for the APVC.

[6] The eruptive activity during the APVC flare-up was episodic, with eruptive volume peaks, during which several ignimbrites were erupted over a short time span, at approximately 8.4, 5.6, and 4 Ma [*Salisbury et al*., 2011]. High-precision $^{40}Ar/^{39}Ar$ dating can distinguish between these ignimbrites if several samples are dated but, in many cases, individual samples yield dates whose analytical precision (typically in the range of tens of thousands of years; *Salisbury et al*., 2011) does not allow confident distinction among ignimbrites (e.g. Table 1 of *de Silva and Gosnold*, 2007). In such cases, determination

Table 1. Characteristic Remanent Magnetization Directions for 45 sites in Central Andean Ignimbrites

Site	Ignimbrite	Latitude (S)	Longitude (W)	Altitude (masl)	Dec	Inc	α_{95}	k	n/N	$J_o(10^{-4}$ A/m)
BL1	Panizos	22.00572	66.55378	4326	70.0	−32.9	5.4	200.1	5/11	16.90
BL2	Panizos	21.98408	66.54904	4253	44.6	−62.6	3.4	231.6	9/9	2.33
BL3	Panizos	22.08486	66.63366	4352	39.3	−36.7	10.0	22.0	11/11	0.72
BL4	Panizos	22.26302	66.84422	4489	50.8	−52.8	8.9	47.3	7/11	0.34
BL5	Panizos	22.36884	66.82402	4391	48.0	−58.6	4.2	178.0	8/9	0.05
BL6	Vilama (no resurgence)	22.20771	66.98247	4547	347.6	−2.0	4.9	189.4	6/9	3.98
BL7	Vilama (no resurgence)	22.22454	67.10605	4475	23.1	−5.6	8.2	67.3	6/6	0.43
BL8	Vilama (resurgence)	22.39173	66.99537	4601	198.6	41.3	4.7	204.0	6/10	28.00
BL9	Vilama (resurgence)	22.39180	66.99653	4629	190.5	15.5	6.6	44.0	12/12	7.10
BL10	Vilama (resurgence)	22.38723	66.99306	4654	22.1	−16.7	17.7	10.7	8/9	25.90
BL11	Vilama (resurgence)	22.38702	66.99236	4635	54.1	6.1	10.9	20.6	10/11	0.82
BL12	Tara	22.38096	67.12437		347.2	69.4	7.4	30.0	14/15	0.29
BL13	Tara	22.43861	67.37691	4539	125.8	−37.2	63.2	1.6	9/9	119.17
BL14	Tara	22.43943	67.37543	4595	254.0	−23.9	9.0	56.5	6/9	209.50
BL15	Guacha	22.43825	67.37601	4588	195.3	60.8	20.8	11.3	6/12	6.65
BL16	Guacha	22.36107	67.39630	4401	179.7	61.9	7.4	48.8	9/12	3.98
BL17	Laguna Colorada	22.36035	67.39832	4418	119.1	−32.4	4.6	213.0	6/6	4.45
BL18	Laguna Colorada	22.35747	67.39884	4414	184.3	−37.4	25.8	4.9	9/9	19.28
BL19	Vilama (no resurgence)	22.25011	67.34529	4233	354.3	13.7	3.5	370.7	6/12	1.64
BL20	Guacha	22.24612	67.30650	4317	139.1	70.9	10.4	42.5	6/12	20.20
BL21	Tara	22.77396	67.12144	4544	346.5	−29.3	10.1	27.2	9/12	11.28
BL22	Tara	22.83261	67.13439	4473	337.6	−27.6	2.7	262.9	12/12	0.18
BL23	Tara	22.87331	67.16188	4477	304.5	−4.2	53.3	1.6	12/12	4.98
BL24	Tara	22.84949	67.14338	4451	334.1	−19.9	3.9	124.5	12/12	0.19
BL25	Guacha	22.77148	67.08501	4535	203.8	69.0	6.6	61.9	9/12	0.13
BL26	Puripica Chico	22.60813	67.58129	4554	141.5	41.9	4.9	189.7	6/6	
BL27	Laguna Colorada	22.22236	67.41368	4452	350.1	−45.8	2.5	913.1	5/6	12.83
BL28	Laguna Colorada	22.27532	67.71793	4364	346.2	−47.0	4.0	275.4	6/6	9.93
BL29	Tatio	22.34629	67.79200	4726	324.5	−37.8	5.9	435.4	3/6	40.00
BL29	Tatio	22.34629	67.79200	4726	11.5	−15.8	5.0	608.0	3/6	40.00
BL30	Guacha	22.25327	67.33435	4219	162.6	79.2	6.9	77.0	7/9	1.02
BL31	Guacha	21.84078	67.33678	4026	174.5	63.4	5.6	86.4	9/9	2.25
BL32	Vilama (no resurgence)	21.84087	67.33619	4026	1.4	20.3	3.5	220.6	9/9	4.67
BL33	Pastos Grandes	21.75059	67.48369	4039	0.1	−18.1	9.2	28.8	10/12	6.08
BL34	Pastos Grandes	21.72769	67.95507	4526	2.6	−15.2	3.9	156.4	10/13	20.50
BL35	Pastos Grandes	21.95883	67.85062	4698	7.4	−21.4	2.8	406.6	8/16	17.17
BL36	Pastos Grandes	21.90072	67.66755	4573	56.4	−71.8	6.7	133.2	5/12	164.67
BL37	Pastos Grandes	21.50216	67.85970	4517	8.2	−20.6	3.1	272.7	9/11	11.83
BL38	Chuhuilla	21.25095	68.12456	3731	188.6	39.5	2.7	314.8	10/15	11.22
BL39	Chuhuilla	21.39199	67.70226	4010	181.9	25.8	2.8	331.3	9/15	9.75
BL40	Pastos Grandes	21.50818	67.61046	4133	9.2	−24.7	2.9	306.7	9/9	4.78
BL41	Alota	21.48675	67.59747	4080	26.8	18.1	6.5	107.7	6/9	8.43
BL42	Chuhuilla	21.45648	67.64257	3795	186.0	14.3	2.4	360.5	11/11	11.50
BL43	Alota	21.43480	67.63180	3758	16.7	−25.6	5.8	80.6	9/9	1.98
BL44	Pastos Grandes	21.44631	67.64776	3892	12.5	−23.7	5.6	85.0	9/9	11.33
BL45	Alota	21.42457	67.64517	3893	17.4	−13.1	9.4	67.8	5/9	12.17

of the characteristic remanent magnetization can provide an effective way to rapidly distinguish among ignimbrites.

[7] Paleosecular variation of the geomagnetic field can result in the acquisition of distinct remanence directions in volcanic units after periods as short as several decades [*Champion and Donnelly-Nolan*, 1994]. Longer periods result in more readily distinguished variation, and, although precise rates of paleosecular variation vary greatly with time and location [*Vestine et al.*, 1959], rates of 4–10 °/century are common [*Champion and Donnelly-Nolan*, 1994]. Using paleomagnetic techniques, ignimbrites can be better identified and their regional distribution determined. This, in turn, allows for a more confident estimate of the erupted volume and a more accurate time/volume history, in this case for the APVC. The paleomagnetic data can also identify a general age of a rock via magnetic polarity stratigraphy and can help evaluate if a particular area has been tilted or rotated since emplacement and acquisition of its magnetic remanence.

[8] Anisotropy of magnetic susceptibility (AMS) data can aid in the correlation of ignimbrites to their specific sources [e.g. *MacDonald and Palmer*, 1990; *Palmer and MacDonald*, 1999; *Paquereau-Lebti et al.*, 2007; *Petronis and Geissman*, 2009]. AMS data provide information on the physical alignment of magnetic minerals within an ignimbrite, and this proxy for rock fabric may be used to interpret flow directions in the depositing current. AMS can provide a way to distinguish between possible vents that are spatially separated. Thus, source identification using AMS data can buttress correlations based upon remanent magnetism.

[9] We present new magnetic remanence and anisotropy of magnetic susceptibility data for eight ignimbrites sourced from four large calderas (Guacha, Pastos Grandes, Vilama, and Panizos) and two smaller centers (Laguna Colorada and Juvinas) in the central APVC of southern Bolivia (Figure 1, Tables 1–3). We adhere to the stratigraphic nomenclature presented by *Salisbury et al.* [2011]. The paleomagnetic data are used to correlate ignimbrites in the APVC and to determine properties of the pyroclastic density currents that produced the deposits. We identify and correlate ignimbrites and locate their calderas. Because the ages of the ignimbrites are well-determined [*Salisbury et al.*, 2011], paleomagnetic correlation of these ignimbrites can be used in the future to positively identify ignimbrites at other localities, allowing for a better delineation of their areal extent. This very well time-constrained paleomagnetic dataset from the southern hemisphere yields a dual polarity record and reveals that two of the units recorded geomagnetic field excursions. These data may be useful in developing Time-Averaged Field models when combined with data from many other locations. The techniques used here will likely work well in other large ignimbrite provinces, such as the Sierra Madre Occidental of Mexico and the Cappadocia region of Turkey.

1.1. Paleomagnetic Techniques

[10] Both characteristic remanent magnetization (ChRM) and anisotropy of magnetic susceptibility (AMS) data were obtained in this study. ChRM is typically interpreted as the early-acquired primary remanence and may have a high laboratory unblocking temperature or high-coercivity behavior in progressive demagnetization. In the case of the APVC ignimbrites, it is interpreted to record the direction of the Earth's magnetic field at the time of cooling of the ignimbrite, and is thus a thermal remanent magnetization (TRM). It can be used to correlate exposures of ignimbrites and also to evaluate tilting that may have occurred in the APVC since emplacement of these ignimbrites. The technique has

Table 2. Central Andean Ignimbrite Characteristic Remanent Magnetization Data

Ignimbrite	Age (Ma)	Source Caldera	Volume (km^3)	Dec	Inc	α_{95}	k	n/N
Puripica Chico	1.70 ± 0.02 Ma	Guacha Caldera	10	141.5	41.9	4.9	189.7	1/1
Laguna Colorada	1.98 ± 0.03 Ma	Laguna Colorada	60	347.2	−46.3	5.1	2395.4	2/4
Pastos Grandes	2.89 ± 0.01 Ma	Pastos Grandes	1500	6.6	−20.7	4.6	214.9	6/7
Tara	3.49 ± 0.01 Ma	Guacha	800	339.3	−25.7	11.6	113.1	3/7
Alota	5.23 ± 0.01 Ma	Alota Ignimbrite Shield	20	17.1	−19.4	27.6	83.9	2/3
Chuhuilla	5.45 ± 0.02 Ma	Pastos Grandes	1200	185.4	26.6	19.9	39.3	3/3
Guacha	5.65 ± 0.01 Ma	Guacha	1300	178.9	68.8	9.0	56.6	6/6
Guacha (w/ Somoza et al. data)	5.65 ± 0.01 Ma	Guacha	1300	178.0	69.2	5.1	89.5	10
Panizos	6.79 ± 0.02 Ma	Panizos	650	51.5	−49.3	15.1	26.7	5/5
Vilama (non-resurgent)	8.41 ± 0.02 Ma	Vilama	1400	1.5	6.8	22.9	17.0	4/4
Vilama (w/ Somoza et al. data)	8.41 ± 0.02 Ma	Vilama	1400	0.5	14.9	11.0	22.9	9

Table 3. Central Andean Ignimbrite AMS Ellipse Principal Axes and Parameters

	K_1		K_2		K_3		L_{mean}	F_{mean}	P_{mean}	Mean Susceptibility	
Site	D (error)	I	D (error)	I	D (error)	I	X_{max}/X_{int}	X_{int}/X_{min}	X_{max}/X_{min}	(10^{-6} SI)	n
Tara Ignimbrite Sites											
BL12	294 (17)	11 (6)	203 (17)	7 (8)	80 (9)	77 (6)	1.011	1.028	1.039	1410	16
BL14	116 (17)	20 (6)	21 (18)	1 (8)	294 (8)	70 (6)	1.009	1.017	1.025	3110	18
BL21	26 (26)	3 (6)	296 (26)	7 (5)	138 (6)	83 (5)	1.004	1.027	1.032	730	15
BL22	235 (24)	13 (5)	328 (24)	11 (9)	97 (9)	73 (5)	1.007	1.049	1.056	199	15
BL23	265 (19)	15 (8)	359 (20)	17 (18)	135 (19)	67 (9)	1.03	1.065	1.098	594	13
BL24	273 (37)	22 (4)	8 (37)	11 (8)	123 (8)	65 (3)	1.004	1.034	1.038	175	15
Pastos Grandes Sites											
BL33	187 (25)	10 (9)	97 (24)	2 (3)	357 (10)	80 (3)	1.003	1.017	1.02	2340	12
BL34	301 (23)	3 (5)	31 (23)	11 (2)	198 (5)	79 (2)	1.005	1.03	1.034	7360	18
BL35	3 (44)	6 (9)	93 (44)	2 (5)	200 (12)	84 (4)	1.002	1.02	1.022	3870	16
BL36	277 (44)	6 (4)	7 (44)	5 (5)	132 (6)	82 (3)	1.005	1.034	1.039	8500	19
BL40	231 (14)	16 (4)	140 (14)	1 (3)	48 (5)	75 (3)	1.01	1.031	1.041	4680	15
Guacha Sites											
BL15	95 (32)	9 (17)	3 (33)	17 (14)	212 (19)	71 (15)	1.005	1.013	1.017	5020	15
BL16	222 (27)	20 (8)	317 (27)	14 (12)	79 (12)	65 (8)	1.005	1.019	1.024	2220	15
BL20	232 (27)	19 (6)	142 (27)	1 (9)	49 (11)	71 (6)	1.012	1.045	1.057	8090	14
BL25	218 (35)	6 (20)	311 (40)	23 (29)	115 (37)	66 (21)	1.009	1.016	1.025	91	13
BL30	250 (30)	19 (22)	44 (66)	69 (25)	158 (66)	9 (25)	1.008	1.004	1.012	2640	14
BL31	140 (33)	10 (8)	230 (33)	0 (6)	321 (9)	80 (5.5)	1.007	1.051	1.059	3630	14
Laguna Colorada											
BL17	260 (13)	12 (5)	351 (13)	3 (4)	96 (5)	77 (4)	1.006	1.015	1.02	8990	16
BL18	257 (40)	5 (11)	347 (41)	3 (15)	108 (18)	84 (10)	1.003	1.01	1.013	2650	15
BL27	231 (45)	9 (10)	322 (45)	7 (10)	86 (13)	79 (8)	1,004	1.019	1.023	699	15
BL28	115 (27)	16 (7)	24 (27)	3 (9)	282 (10)	74 (7)	1.005	1.017	1.022	1670	14
Vilama											
BL7	192 (22)	16 (9)	96 (25)	18 (14)	321 (19)	66 (9)	1.013	1.053	1.067	387	18
BL8	286 (14)	14 (5)	196 (15)	1 (5)	102 (6)	76 (3)	1.009	1.07	1.08	15100	9
BL9	298 (6)	15 (2)	29 (6)	1 (4)	123 (4)	75 (2)	1.009	1.038	1.048	5350	10
BL10	301 (19)	16 (8)	210)19)	3 (5)	111 (5)	74 (5)	1.011	1.051	1.063	2560	8
BL11	296 (57)	17 (6)	26 (57)	1 (6)	120 (7)	73 (5)	1.006	1.134	1.141	2020	10
BL19	241 (38)	23 (13)	332 (26)	2 (16)	67 (37)	67 (22)	1.011	1.015	1.026	1650	14
BL32	231 (32)	11 (6)	141 (32)	1 (4)	44 (8)	79 (4)	1.004	1.021	1.024	6000	15
Panizos											
BL4	29 (16)	18 (2)	121 (5)	5 (5)	227 (5)	71 (2)	1.006	1.053	1.059	380	18

been widely and successfully used for these purposes [e.g. *Wells and Hillhouse*, 1989; *McIntosh*, 1991; *Lipman et al*., 1996; *Speranza et al*., 2012].

[11] AMS data typically record the partial preferred alignment of ferro- and ferri-magnetic grains within the rock, either as a shape anisotropy, in which anisotropic magnetic grains are oriented within the ignimbrite, or as a distribution anisotropy, in which grains touch or are close to each other, forming alignments of grains, and an anisotropy results from the distribution of those interacting grains [*Hargraves et al*., 1991; *Rochette et al*., 1992]. A theoretical basis for AMS in ignimbrites is presented in *Pioli et al*. [2008] and *Ort et al*. [2003] and references therein. AMS can provide information on the depositional fabric in the ignimbrite, and the elongation of magnetic grains commonly parallels the flow direction. In pseudo-single domain grains of low-Ti magnetite that are common to most ignimbrites, the maximum susceptibility direction (K_1) is parallel to the longest dimension of the grain. The K_1 direction in an ignimbrite is commonly interpreted to be parallel to the flow direction, although cases exist [e.g. *Ort et al*., 1999] in which it has been interpreted as perpendicular to flow in proximal deposits. These proximal deposits appear to be produced by rapid sedimentation from an expanded, but condensing, flow (e.g. a deflation zone). In distal deposits from dense pyroclastic currents, K_1 directions are typically consistent with independently inferred flow-parallel directions [e.g. *Ort*, 1993; *Somoza et al*., 1994]. The magnetic fabric is typically flattened in ignimbrites, due to both depositional and post-depositional compaction processes, and orientation of the AMS foliation can

provide an indication of post-depositional tilting in some cases. Topography can influence the flow direction [*Baer et al*., 1997; *Ort et al*., 2003], so simple triangulation to identify the source vent for an ignimbrite is possible only in areas of subdued topography.

1.2. Previous Paleomagnetic Studies in the APVC

[12] Most paleomagnetic studies in the Altiplano and Puna area have focused on determining the magnitude and sense of rotation associated with the development of the Bolivian orocline [e.g. *Somoza et al*., 1996, 1999; *Prezzi*, 1999; *Coutand et al*., 1999; *Roperch et al*., 2000; *Lamb*, 2001; *Prezzi and Alonso*, 2002; *Beck*, 2004; *Richards et al*., 2004; *Rousse et al*., 2005; *Barke et al*., 2007; *Taylor et al*., 2007]. These studies reveal different time periods and kinematics associated with the rotations involved in forming the Bolivian orocline. Nevertheless, these rotations occurred by early Miocene time and little to no rotation has been documented for the 10 to 1 Ma time period of interest in this study. Few studies have used paleomagnetic data to characterize different central Andean ignimbrites [e.g. *Somoza et al*., 1996; *Paquereau-Lebti et al*., 2007] or AMS data to estimate vent locations [*Ort*, 1993; *Somoza et al*., 1994; *Paquereau-Lebti et al*., 2007]. These studies focused on a small number of ignimbrites and demonstrated that the technique can be applied to central Andean ignimbrites.

1.3. Eight Studied Ignimbrites

[13] The eight ignimbrites studied in this project are the Vilama Ignimbrite (8.41 Ma; Vilama Caldera), Cerro Panizos Ignimbrite (6.86 Ma; Cerro Panizos Caldera), Guacha Ignimbrite (5.52 Ma; Guacha Caldera), Chuhuilla Ignimbrite (5.45 Ma; Pasto Grandes Caldera), Alota Ignimbrite (5.23 Ma; Alota Ignimbrite Shield), Tara Ignimbrite (3.49 Ma; Guacha Caldera), Pastos Grandes Ignimbrite (2.89 Ma; Pastos Grandes Caldera) and Laguna Colorada Ignimbrite (1.98 Ma; Laguna Colorada Ignimbrite Shield) (Figure 1; all ages from *Salisbury et al*., 2011). The Puripica Chico Ignimbrite (1.70 Ma, Guacha Caldera source) and Tatio Ignimbrite (0.70 Ma, Tatio Ignimbrite Shield) were each sampled at only one site. The eight main ignimbrites comprise the dominant upper Miocene volcanic rocks of the APVC in southern Bolivia. A total of 45 sites were sampled (Table 1; Figure 1).

2. Methods

[14] Sampling in the field was carried out in October, 2007, using existing maps and satellite imagery to locate sites. All sites are in surface outcrops, as no roadcuts or quarries were found. Cylindrical samples were drilled with a portable gasoline-powered rock drill and oriented using both magnetic and sun compasses. Because many of the rocks sampled are poorly lithified, water flow and rotation speed of the drill were managed so as to produce the least amount of sample erosion as possible. We do not see a systematic or larger error in the sites with soft samples.

[15] Eight to 18 independently oriented samples were collected per site and were cut into 22-mm-tall, 25.4-mm-diameter cylinders (specimens) for analysis. Specimens from sites for which AMS data were desired were first analyzed on an AGICO Kappabridge KLY-2 at the Laboratori de Paleomagnetisme de Barcelona. A total of 419 specimens from 29 sites were analyzed for AMS. Susceptibility was measured in fifteen different orientations for each specimen and the data reduced using the Ani20 program and analyzed using the ANISOFT (both from AGICO) and PmagPy-2.51 (written by L. Tauxe, University of California San Diego) programs.

[16] Remanence was measured on 471 specimens from the 45 sites, using different analytical approaches. To start, six specimens from each site (except BL26) were analyzed at the Laboratori de Paleomagnetisme de Barcelona. Specimens were stepwise demagnetized using a Magnetic Measurements MMTD-80 thermal demagnetizer in batches of 80 specimens. After cooling in a negligible magnetic field inside the instrument, specimens were kept in mu-metal boxes between measurements. Specimens were analyzed on a 2G SRM 755R cryogenic superconducting rock magnetometer. Changes in bulk susceptibility with progressive demagnetization were monitored with a Kappabridge KLY-2.

[17] For site BL26, the remanence was too strong to be measured on the 2G magnetometer, so specimens were analyzed using thermal demagnetization at the Alpine Laboratory of Paleomagnetism in Peveragno, Italy. These six specimens were stepwise demagnetized with a Schonstedt TSD-1 thermal demagnetizer and analyzed on an Agico JR-6 Dual Speed spinner magnetometer using REMA6 software. Changes in bulk susceptibility with respect to demagnetization temperature were monitored with an AGICO Kappabridge KLY-3.

[18] Three to nine specimens from each site were analyzed in the Northern Arizona University paleomagnetism laboratory. Specimens were partially stepwise demagnetized using a Molspin shielded alternating field (AF) demagnetizer in fields to 100 mT, and analyzed on a Molspin minispin magnetometer.

[19] Principal component analysis was used to determine the directions and relative intensities of the components of magnetization. Data from specimens that did not show a progression toward the origin on *Zijderveld* [1967] diagrams or did not show >70% demagnetization at 630 °C or 100 mT were discarded as unreliable because of uncertainty over whether the ChRM had been identified. Data were then analyzed using the Remasoft (AGICO) and PMGSC programs (R. Enkin, Geological Survey of Canada). We combined the results from the thermal and AF demagnetization experiments to produce the estimated site ChRM mean directions, and these were then combined for each ignimbrite ChRM direction. Sites with poor clustering of specimen directions or site directions that were more than 60º from the others were not used for determining the ignimbrite ChRM directions.

3. Results

3.1. Magnetic Characteristics

[20] The response to progressive stepwise thermal demagnetization tended to be similar at the within–site level (Figure 2). Specimens from a few sites show complete unblocking of remanence by 580 °C (T_b, or maximum unblocking temperature, of magnetite), but many specimens retained significant fractions of their natural remanent magnetization (NRM) at higher temperatures, with a few retaining more than 10% of the NRM at 680 °C. Typically, specimens display the broadest range of unblocking between 570 and 625 °C. In nearly all these cases, the remanence direction remained consistent with further unblocking above 570 °C, until the NRM was completely unblocked and the remaining remanence displayed a random direction. This distribution of laboratory unblocking temperatures, common in many ignimbrites, may be a result of high-temperature oxidation shortly after emplacement of the ignimbrites [e.g. *Wells and Hillhouse*, 1989] or of low-temperature oxidation of magnetite to form maghemite. High-temperature oxidation can cause titanium to exsolve from the spinel lattice of titanomagnetite, forming lamellae of ilmenite and leaving magnetite with a 580 °C Curie temperature. This oxidation can also produce titanohematite, with Curie temperatures exceeding 630 °C, which is observed in some specimens. Low-temperature oxidation of magnetite forms maghemite, which, during thermal demagnetization, can form hematite [*Dekkers* 2009].

[21] Bulk susceptibility, monitored during thermal demagnetization, shows that most specimens exhibit little variation or a small yet consistent increase or decrease in susceptibility with progressive demagnetization. All samples show a decrease in bulk susceptibility between 500 and 570 °C. Many sites show peaks in susceptibility, or reach a plateau, around 300 °C. Several sites with high initial susceptibilities show drops in susceptibility to 25% of the initial values by 650 °C, suggesting that the mineral responsible for the high initial susceptibility is not stable at elevated temperatures.

[22] Response to alternating field demagnetization produces simpler patterns, with a steady decay toward the origin on orthogonal projection plots and generally improved clustering of directions above 20 mT peak field in comparison to thermal demagnetization (Figure 3). The remanence directions measured for specimens from the same site are similar for the higher laboratory unblocking temperature and higher alternating field steps, suggesting that ChRM values are adequately identified in demagnetization.

[23] Because of the high altitude, lack of vegetation, and slow erosion rate in the APVC, lightning strikes are an important consideration in sampling [e.g. *Tauxe et al*., 2003]. Many sites appear to have been affected by lightning strikes, with samples showing univectorial decay of randomly oriented magnetizations during thermal demagnetization, but more consistent remanence directions during AF demagnetization. The high-intensity lightning-induced component was randomized at low peak AF demagnetization steps, and higher peak fields isolated a more consistent direction of magnetization interpreted as the ChRM. These directions from AF demagnetization also tended to have good within-site agreement.

3.2. Characteristic Remanent Magnetization

[24] All but six of the 45 sites have α_{95} confidence estimates below 10º, with 32 sites having α_{95} values between 2.5 and 7.5º (Table 1, 2; Figure 4). The median α_{95} for all 45 sites is 5.7º. As described above, the sites are all exposed natural outcrops

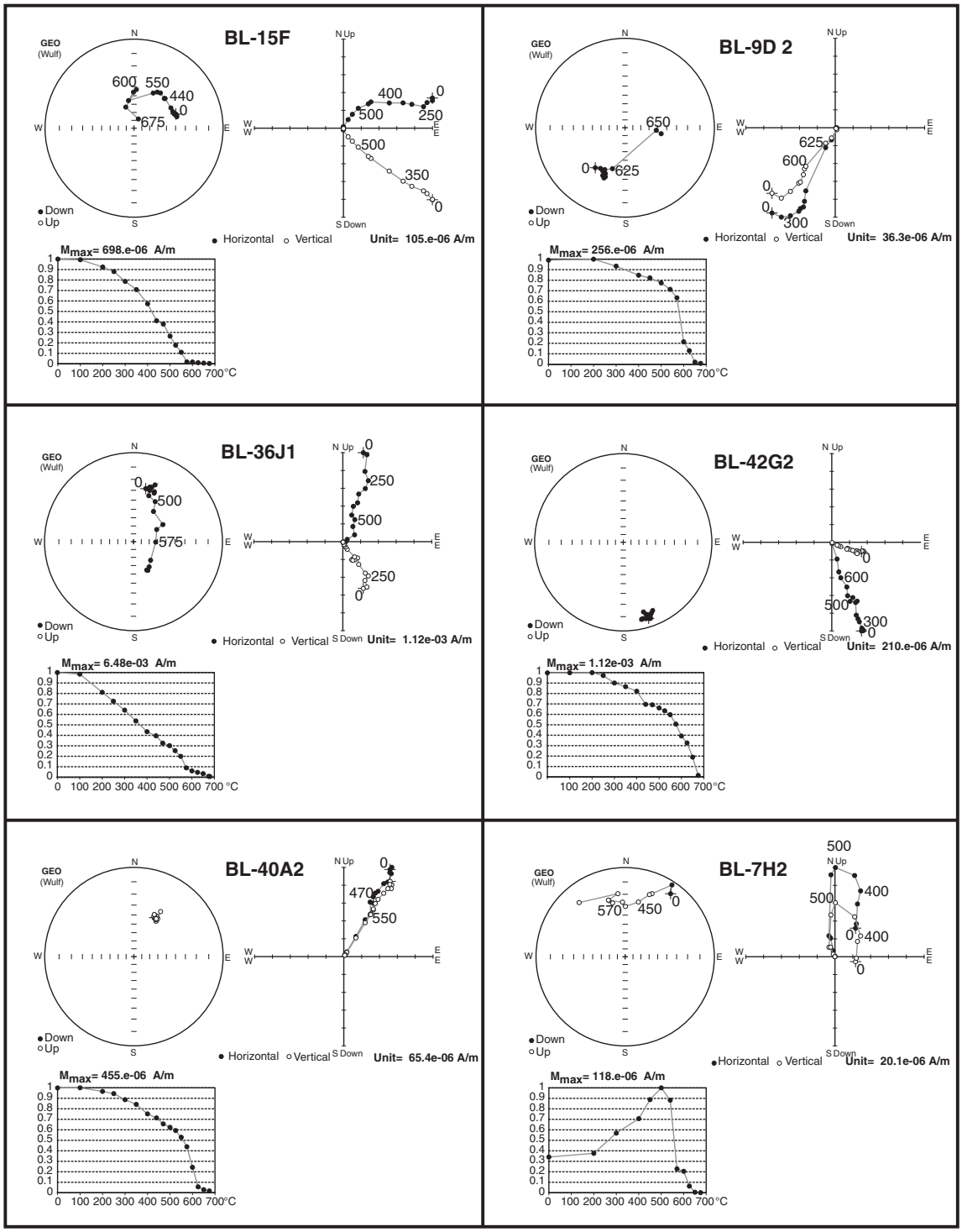

Figure 2. Thermal demagnetization data for representative specimens from the APVC. For each specimen, equal area stereonet and Zijderveld (1967) diagrams are shown. For each specimen, the upper left plot is an equal area projection, the lower left is an orthogonal plot, with numbers representing temperature in °C, and the lower right is a normalized intensity decay curve.

rather than fresh road cuts or quarries. No correlation between the lithification of the outcrop or the particular ignimbrite and the magnitude of the α_{95} values was apparent in the data. Although the Tara Ignimbrite has two sites with very large α_{95} values, it also has sites with very little dispersion. Another way to check for possible errors in sampling and orientation is by comparing the ChRM and AMS

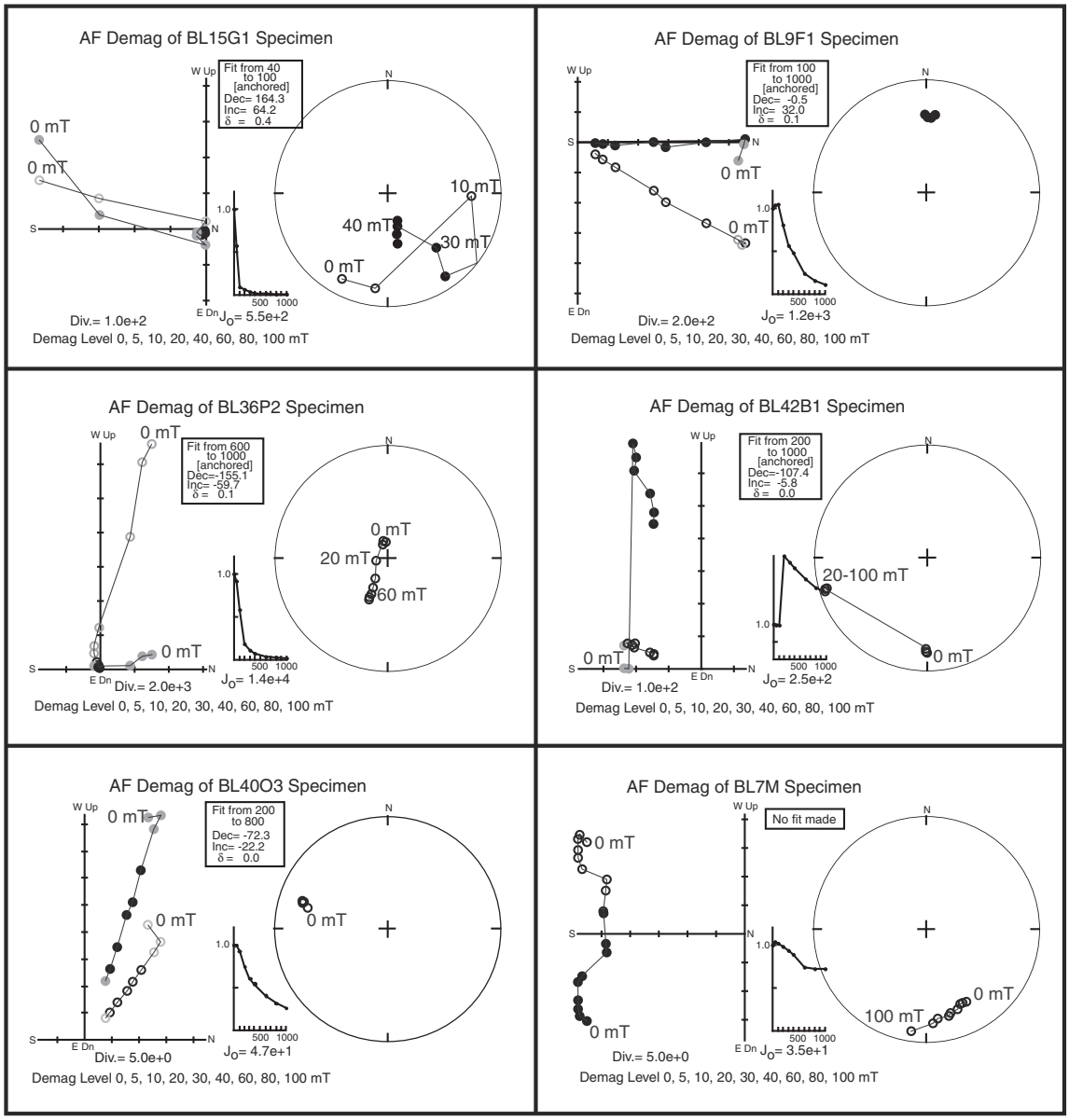

Figure 3. Alternating Field (AF) demagnetization data for representative specimens from the APVC (note that the specimens are from the same sites as those of figure 2). For each sample, equal area stereonet and Zijderveld (1967) diagrams are shown. For each sample, the left plot is an orthogonal plot, the right plot is an equal area projection, and the center plot is a normalized intensity decay curve.

data (Tables 1, 3). Large dispersion in ChRM does not correlate with dispersion in the AMS data. For example, the Tara site BL23 has one of the largest α_{95} values in the study, yet the AMS error ellipses are in the middle of the range for that ignimbrite. We interpret this to indicate that the high within-site dispersion in ChRM is not caused by errors in orientation, but is related to factors intrinsic to the rocks. We consider the site α_{95} confidence estimates and the *k* (dispersion parameter) values to indicate that the site mean ChRM directions are reasonable estimates of the geomagnetic field.

[25] The between-site dispersion of ChRM directions for each ignimbrite is greater than the observed within-site dispersion. The ignimbrite median α_{95} value is 9.0º. For three ignimbrites (Tara, Alota, and Chuhuilla), this is at least partly due to a low number of sites used in the calculation of the ignimbrite ChRM. Several Tara sites had anomalous site mean directions, and several sites originally thought to be from the Alota and Chuhuilla ignimbrites proved to be from other ignimbrites, leaving fewer sites with which to calculate the unit mean direction. The ChRM values

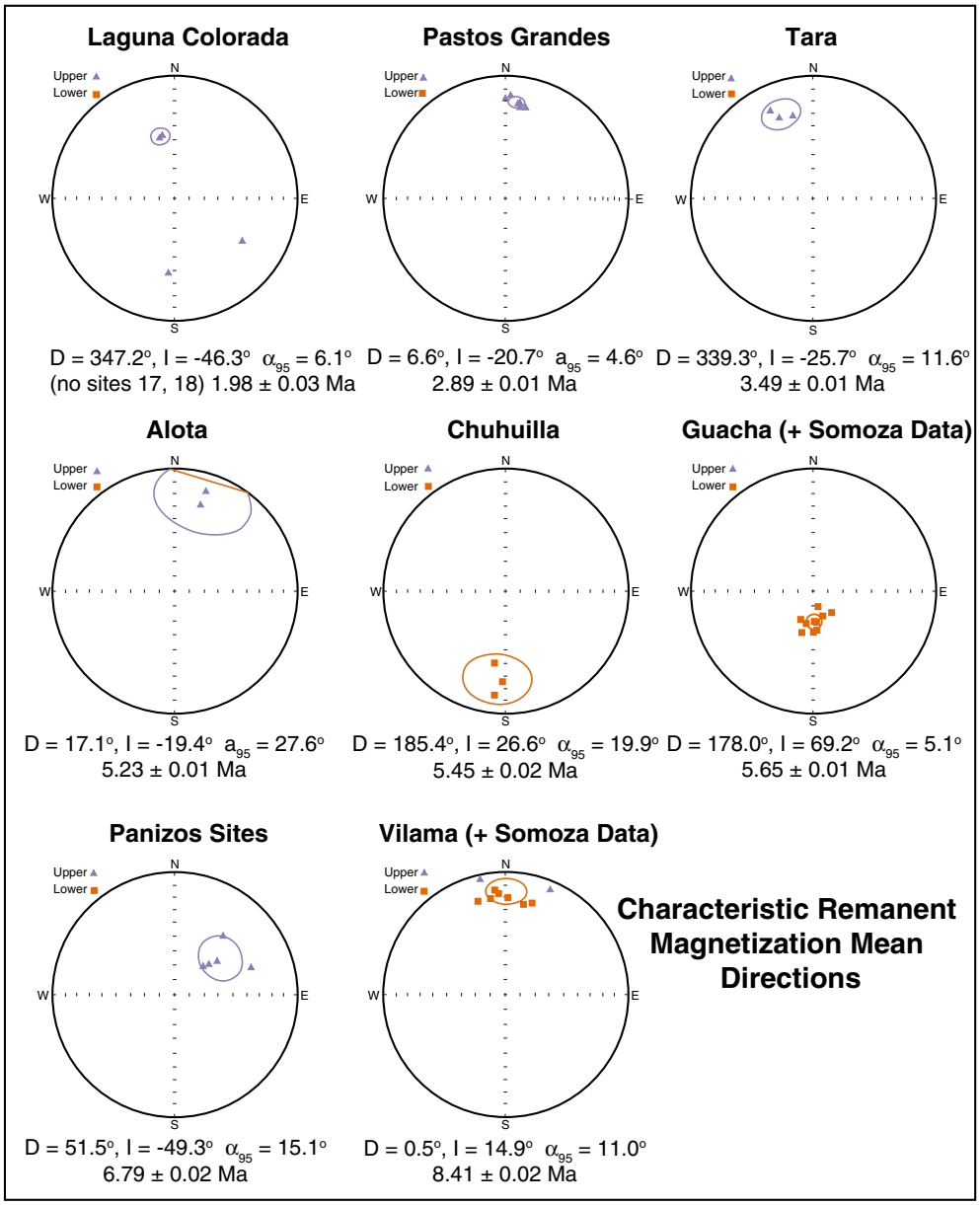

Figure 4. ChRM directions for each ignimbrite, showing the estimated site mean directions calculated using all accepted sites.

for Pastos Grandes and Guacha ignimbrites show the least dispersion and are likely the best defined.

[26] NRM intensity data were plotted against initial bulk susceptibility to determine if the magnetic properties of the APVC ignimbrites are characteristic. Some ignimbrites, such as Chuhuilla and Panizos, have distinctive data clusters, but others, such as Pastos Grandes and Alota, show wide ranges of values, while a few (e.g. Guacha, Tara, Vilama) cluster well except for one or two outlier sites. This combination of parameters cannot be used to confidently distinguish between different ignimbrites.

3.3. Anisotropy of Magnetic Susceptibility

[27] AMS data were obtained primarily from sites with locations chosen to triangulate the vent areas for selected ignimbrites. Because of this, the directions of the K_1 (maximum susceptibility) axes are the primary concern. However, other AMS characteristics must be considered to interpret the AMS data. An average of 15 specimens per site were analyzed for AMS (Table 3; Figure 1X, Supplementary Material in Data Repository). The average degree of anisotropy (P) for all sites is 1.04. All but one site (BL30, Guacha Ignimbrite) have oblate AMS

ellipsoids, indicating that the foliation (F) defined by the K_1 and K_2 axes dominates the K_1 lineation (L). The average L value is less than 1.01. In spite of this, the specimen K_1 values group moderately well for most sites, with error ellipses in the 20-30º range.

[28] The AMS K_1 directions, plotted on a digital elevation map of the central APVC, aid in identifying vent areas for the ignimbrites (Figure 5). In some studies of the deposits of high-mobility pyroclastic flows [e.g. *Fisher et al.*, 1993; *Baer et al.*, 1997; *Ort et al.*, 2003; *Pioli et al.*, 2008], the plunge of the K_1 vector with respect to the base of the ignimbrite is interpreted to be an imbrication and thus the direction of the K_1 vector indicates the up-flow direction. The map pattern of K_1 directions at the sampled sites (Figure 5) varies. Some ignimbrites (e.g. Guacha, Pastos Grandes, and Laguna Colorada) have site K_1 trends and plunges that are consistent with radial flow from the vent, but in other cases, especially at more distal locations, the plunge directions are not consistent with flow from the inferred vent. In a few cases, the plunge is shallow and the error ellipses permit the opposite direction for the plunge. In other cases, topography or unsteady deposition may lead to opposite plunge direction. A consistent and interpretable imbrication of the K_1 axis does not appear in the APVC ignimbrites, as also suggested by *Ort* [1993] for the Panizos Ignimbrite, so we treat the K_1 directions as trends with no directional sense.

4. Discussion

4.1. Paleomagnetism

[29] The identification of the ChRM of the APVC ignimbrites is a major goal of this study. Despite the lack of fresh roadcuts or quarries to sample, the within-site data are generally of good quality. This suggests that the estimated site mean directions are representative of the ChRM for the rocks of that location. The higher ChRM dispersion for the ignimbrites (between-site errors), compared to the site ChRM error ellipses (within-site errors), warrant discussion. The between-site dispersion is higher for the Guacha, Chuhuilla, Panizos, and Vilama ignimbrites (Table 2) than their typical site-level dispersion (Table 1). On the other hand, the estimated mean

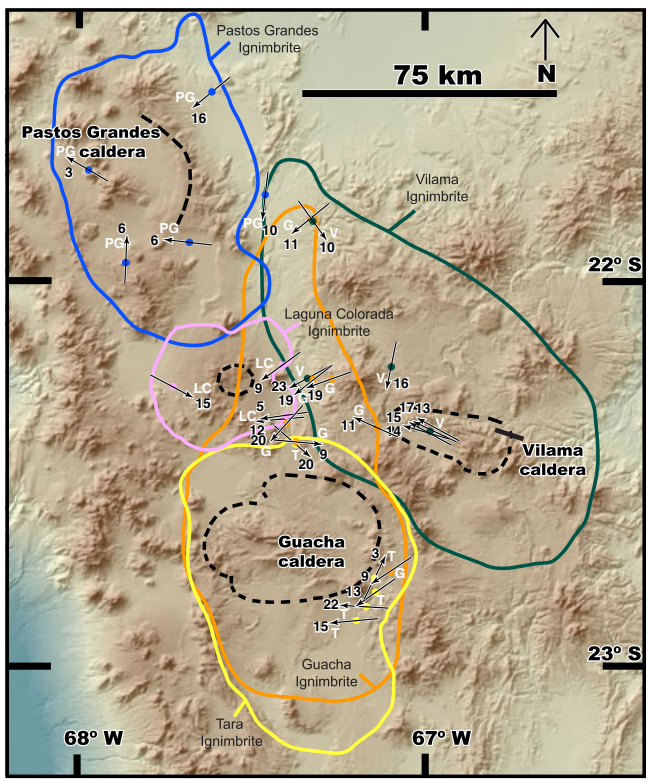

Figure 5. AMS K_1 directions plotted on a DEM of the APVC. Outcrop extents of the ignimbrites are marked by color lines, each labeled with its ignimbrite. The arrows on the figures indicate the trend of the K_1 vector and the number by the arrowhead indicates the plunge value in the direction of the arrow. White letters, placed as close as possible to the arrowhead, indicate the sampled ignimbrite (G = Guacha, LC = Laguna Colorada, PG = Pastos Grandes, T = Tara, V = Vilama) and the dots in the centers of the arrows are also keyed by color to the ignimbrites to which they correspond.

direction for the two youngest large ignimbrites, Pastos Grandes and Tara, is better defined than those of their individual sites, which is the anticipated case if the ChRM was acquired instantaneously and the rock has not been deformed since. One possible explanation for some of the scatter in directions is that deformation and/or tumescence and detumescence events associated with the calderas caused differential rotations among sites. Too few sites are included in this study to fully assess these possibilities. The diminished scatter within the younger ignimbrites, which should have experienced less caldera-related activity since their emplacement, is consistent with this hypothesis. The younger ignimbrites were also likely emplaced on more subdued topography as a result of deposition from earlier flows.

[30] Several observations are inconsistent with the dispersion of ignimbrite ChRM directions being caused by tilting or rotation of the ignimbrites. Most tectonic activity on the plateau appears to have ceased before emplacement of the ignimbrites we examined [cf. *Barke et al*., 2007], but it is possible that a modest amount occurred locally, enough to add scatter to the data without revealing a consistent pattern. Little tilting appears to have taken place, as the ignimbrite basal contacts are typically close to horizontal. The dispersion in the ignimbrite ChRM data is in both declination and inclination, so neither simple rotation nor tilt is a sufficient explanation for all of the data. Detumescence after the emplacement of the ignimbrites could have resulted in now-horizontal strata that were originally more steeply dipping. If such a process occurred during the cooling of the ignimbrites, especially during the early stages at higher temperatures during magnetization blocking, it could result in some scatter to the ChRM directions that would be difficult to identify, and the magnitude of tilting would vary with location and timing. All of our AMS data yield near-horizontal foliations, which implies tilting, if it took place, was $<10^{o}$, which is also the range of observed within-unit scatter.

[31] Paleosecular variation of the magnetic field during cooling of the individual ignimbrites [e.g. *Hagstrum et al*., 1982; *Lipman et al*., 1996] may be a more likely explanation for the dispersion of ignimbrite ChRM values. *Wells and Hillhouse* [1989] showed that thicker sections of the Peach Springs Tuff have distinct remanence directions with steep inclinations. In the interiors of >60-m-thick deposits, where cooling would be expected to be slower, the ChRM directions are much steeper than at the top and bottom of the deposit, where directions match those of thinner, more quickly cooled deposits. They interpret these observations as reflecting secular variation during the cooling of the ignimbrite. A similar explanation may apply to the APVC ignimbrites we sampled. Welding of the ignimbrite at some sites indicates high temperatures of emplacement and there is a wide range in thickness of the ignimbrites at the sampled outcrops. Consequent prolonged (on the order of a century; *Riehle*, 1973) cooling in thicker sections could have led to sites cooling through the blocking temperature range and being subject to vapor-phase crystallization of magnetic minerals over different time intervals. One approach to address this issue in future studies would be to only sample the quickly cooled base of the ignimbrite.

4.2. Correlation of Ignimbrites

[32] The ChRM data are sufficiently distinct for each ignimbrite to facilitate correlation of the ignimbrites. Several of the APVC ignimbrites occupy similar stratigraphic levels but their ChRM directions are distinct (Table 2, Figure 4). Two ignimbrites that erupted at about 3 Ma, the Pastos Grandes and Tara ignimbrites, can be differentiated because their ChRM directions have an angular separation of 25º, well outside the error (7º) between their directions. Three ignimbrites that erupted between 5.6 and 5.3 Ma, the Alota, Chuhuilla, and Guacha ignimbrites, yield distinct ChRM directions (Alota to Chuhuilla angular separation is 169º, Alota to Guacha angular separation is 130º, and Chuhuilla to Guacha angular separation is 42º, with combined errors between them of 10 – 14º). The two oldest ignimbrites, the Panizos and Vilama ignimbrites, are also clearly distinguishable (angular separation of 78º with a combined error of 13º). The 2.89-Ma Pastos Grandes and 5.23-Ma Alota ignimbrites are the only two whose ChRM directions are statistically indistinguishable (angular separation is 9º and their combined error is 9º), but, although their deposit distributions overlap in some areas, they are different enough in age to be identified by stratigraphic position. They are also distinguished by lithologic and petrologic characteristics [*Salisbury et al*., 2011]. Therefore, the new ChRM data can be used to correlate ignimbrites in the APVC.

[33] We used ChRM directions to determine the previously uncertain identity of an ignimbrite in five cases. ChRM data confirm that the ignimbrite at sites BL20 and BL31 (Figure 1) is the 5.65 Ma Guacha ignimbrite. BL20 was mapped as Guacha due to outcrop continuity and stratigraphic position,

but had yielded a spurious 6.3 Ma date [*Salisbury et al*., 2011] that did not match any known ignimbrite. BL31 is an isolated exposure lacking continuity, but stratigraphically could correlate with either the Guacha or Chuhuilla ignimbrite. At BL25, the Guacha ignimbrite at the site had been misidentified previously as Tara ignimbrite, but the distinctive ChRM allowed its positive identification. BL33, which could have been either the Pastos Grandes or Guacha ignimbrite, failed to yield a date after several attempts, but the ChRM direction is clearly that of Pastos Grandes ignimbrite. At BL37, the ignimbrite was identified as Chuhuilla, but ChRM data confirmed a correlation with Pastos Grandes, an interpretation that was subsequently borne out by a closer analysis of the satellite imagery. The data from these sites have been included with existing data to provide an enhanced data set. This does not significantly change the directions but does decrease dispersion slightly (Figure 4; Table 2).

[34] One paleomagnetic result that prompts further research is from site BL12. This isolated exposure was thought to be the Tara Ignimbrite, but its ChRM direction is unlike that from other Tara Ignimbrite sites. The site mean has moderate dispersion ($\alpha_{95} = 11.6^o$, $k = 113.1$), but is reversely magnetized and cannot be Tara Ignimbrite. It is about 30º from the Guacha Ignimbrite ChRM direction, so if it is the Guacha Ignimbrite, it has been rotated. Because Tara and Guacha ignimbrites have similar areal distributions and appearance in this particular sector, it is difficult to distinguish them. An age determination or more intensive field study would resolve this issue.

[35] A counterpoint to these paleomagnetic success stories is provided by data from site BL44. The ignimbrite at this site was originally mapped as Alota ignimbrite, but further stratigraphic work and mapping allowed us to identify it as Pastos Grandes ignimbrite. Because the two ignimbrites have ChRM directions that are statistically indistinguishable, the paleomagnetic data were not useful in distinguishing between the two possible ignimbrites. This identification error, coupled with the poor quality of site BL41 ChRM data, leaves only two sites to estimate the Alota Ignimbrite ChRM direction. An accurate ChRM direction for the Alota ignimbrite cannot be determined without more sites. This example illustrates 1) the importance of using multiple lines of evidence to identify the ignimbrite sources and 2) the necessity of knowing the error ellipses for the ChRM directions. These examples confirm the utility of using paleomagnetic data to correlate ignimbrites in areas with many overlapping units, and the mean ChRM direction for a given ignimbrite is best defined by a large number of sites from non-deformed localities.

[36] Two ignimbrites sampled in this study were also studied by *Somoza et al*. [1994, 1996]. Our ChRM values (Table 2) for the Vilama Ignimbrite ($D = 1.5$, $I = 6.8$, $\alpha_{95} = 22.9$, $n = 4$), which has the greatest dispersion of the ignimbrites we studied, are within errors of theirs ($D = 359.7$, $I = 21.3$, $\alpha_{95} = 12.5$, $n = 5$). They also sampled what they identified as the Atana ignimbrite, following the work of *Gardeweg and Ramírez* [1987]. *Lindsay et al*. [2001] subsequently showed that ignimbrites previously mapped as Atana to the northeast of La Pacana caldera (the area sampled by *Somoza et al*.) were either Tara (3.64 Ma) or Guacha (5.65 Ma) ignimbrites [see also *Salisbury et al*., 2011]. In this light, it is interesting that *Somoza et al*.'s [1994, 1996] ChRM direction for the Atana Ignimbrite ($D = 176.7$, $I = 69.8$, $\alpha_{95} = 5.7$, $n = 4$) is statistically indistinguishable from our mean for the Guacha Ignimbrite ($D = 178.9$, $I = 68.8$, $\alpha_{95} = 9.0$, $n = 6$), but very different from the Tara Ignimbrite ($D = 339.3$, $I = -25.7$, $\alpha_{95} = 11.6$, $n = 3$). We suspect that their Atana ChRM data are actually from the Guacha Ignimbrite. This further highlights the need for a ChRM database for the APVC ignimbrites.

[37] As with our data, *Somoza et al*.'s [1994, 1996] estimated dispersion of the ChRM for the Vilama Ignimbrite is much larger than the dispersion values for each of their five sites, and the overall α_{95} value for their Atana Ignimbrite (now identified as Guacha Ignimbrite) is similar to, rather than smaller than, the α_{95} values for each of their four sites. This is further evidence that large α_{95} values are a characteristic of the ignimbrites and not the result of poor sampling or analysis techniques.

[38] This study shows that the error associated with ChRM is an important part of the identification of these ignimbrites and that the errors may not decrease significantly with an increased number of site mean determinations. Combining the values obtained by *Somoza et al*. [1994, 1996] and our study, which together provide 9–10 independent sites per ignimbrite, we conclude that 5-7º α_{95} error ellipses may be typical of these ignimbrites, and additional site mean data may only reduce the ignimbrite dispersion values to this magnitude. The observed dispersion is an indication of the range of values to expect for at least some ignimbrites, which show dispersed ChRM directions, rather than a single direction acquired from instantaneous cooling.

The measured ChRM direction at any given site may lie 5-10º away from the mean ChRM direction because of geologic processes and analytical errors may contribute to this dispersion.

[39] The polarity of all ChRM directions from the ignimbrites is consistent with the geomagnetic polarity timescale [*Walker and Geissman*, 2009] except for the oldest and easternmost ignimbrites, the Panizos and Vilama ignimbrites. Both of these have what are typically referred to as "transitional" directions – the Panizos ChRM points steeply up and eastward and Vilama is shallow and directly north. They may record cooling during magnetic excursions or short-lived polarity events.

4.3. Anisotropy of Magnetic Susceptibility

[40] The AMS data (Figure 5; Table 3) help in identifying the sources of the Pastos Grandes and Laguna Colorada ignimbrites (the Pastos Grandes caldera and Laguna Colorada shield, respectively). K_1 directions from the two ignimbrites triangulate to define their vent areas (Figure 5). Some of the K_1 directions from the Guacha Ignimbrite are interpreted to define the vent area (within the Guacha caldera), whereas others appear to parallel paleotopography. Paleotopography is generally easy to determine in the APVC as the valleys and mountains present in late Miocene time are still extant and exposed.

[41] Many K_1 directions from the 3.51 Ma Tara ignimbrite are consistent with flow from the Guacha caldera (Figure 5), confirming age data [*Salisbury et al*., 2011] and recent mapping showing that the caldera was the source of both the 2.89 Ma Tara and 5.45 Ma Guacha ignimbrites. Tara pyroclastic flows were probably affected by caldera and pre-caldera topography, with the flow ponding within the pre-existing Guacha caldera moat. A very thick (>200 m) section of Tara Ignimbrite is located at the Argentina/Bolivia/Chile border to the east of the Guacha Caldera, an area now overlain by the Cerro Zapaleri stratovolcano. We are uncertain why it is so thick and lithic-rich in this area. Possible explanations include a pre-existing depression and/or syn-eruptive subsidence outside of the main Guacha caldera.

[42] The K_1 directions from the Vilama Ignimbrite (Figure 5) also appear to follow paleotopography, providing evidence of low mobility that was also found using AMS on the nearby (and similarly aged) Cerro Panizos Ignimbrite [*Ort*, 1993] and in the Cerro Galan Ignimbrite in NW Argentina [*Cas et al*., 2011]. As the oldest of the large ignimbrites of the APVC, the Vilama pyroclastic density currents may have encountered more topography than the later flows. Four sites in the resurgent dome have the same K_1 declinations (within 15º) and plunges of about 15º. The L values are similar to other sites in the Vilama Ignimbrite, but the F (foliation) values are higher, a likely consequence of the extreme welding at these sites. The plunge of the K_1 directions may provide an estimate of the maximum amount of tilting of the ignimbrite by the resurgence, on the order of 15º.

[43] Another technique in the interpretation of AMS fabrics in ignimbrites is to look at the orientation of the K_1/K_2 (foliation) plane [e.g. *Geissman et al*., 2010]. In some cases, this plane has a dip that is not directly down the K_1 axis. The K_3 axis is normal to this plane and indicates the down-dip direction of the plane. The orientation of the K_3 axis helps define possible flow direction in a few cases in the APVC ignimbrites. The BL7 site of the Vilama Ignimbrite yields a K_3 direction that points toward the Vilama resurgent center. The eastern Tara sites (BL21-BL24) produce K_3 directions that are consistent with flow from the Guacha domes area. In many cases from other APVC sites, however, the K_3 mean direction is within 5º vertical and the K_1/K_2 plane is nearly horizontal. In such cases, use of this technique to interpret flow directions cannot be done with confidence as small changes in the foliation orientation can change the K_3 direction significantly. Because of this, we use the K_1 directions for interpretations, but note that the K_3 axis can be used in some cases to check these directions.

[44] AMS K_1 directions are imbricated with respect to the lower contact of some ignimbrites from other volcanoes [e.g. *Baer et al*., 1997; *Palmer and MacDonald*, 1999; *Ort et al*., 2003], but the APVC ignimbrites do not show a clear imbrication. *Ort et al*. [1999] discuss some of the likely origins for K_1 axis orientations. K_1 axes perpendicular to flow may correspond to rolling bedload grains, whereas imbricated K_1 directions may indicate tractional sedimentation from the pyroclastic current. K_1 directions that are parallel to flow, but are not imbricated, may be best explained by tractional deposition from flow in which turbulence is damped by high particle concentrations, perhaps as segments of dense flow stop abruptly.

5. Conclusions

[45] The ChRM directions from the ignimbrites of the APVC examined in this study are, in most cases,

sufficiently distinct to be used for identification of the ignimbrites, especially if the paleomagnetic data are combined with stratigraphic information. Two ignimbrites have directions that are statistically indistinguishable, but their stratigraphic positions are distinct. The dispersion of the ChRM directions at the between-site level is greater than the within-site dispersion. We postulate that this is due to hot emplacement, above the maximum blocking temperature, followed by slow cooling of the thick sections of ignimbrite. Paleosecular variation of Earth's magnetic field was recorded by the rocks during cooling, so that the interiors of deposits may have passed below the ChRM blocking temperature range at a different time than the more quickly cooled bases and tops. AMS data allow the identification of the vent areas for some of the ignimbrites, and also demonstrate that there was little post-emplacement tilting of the ignimbrites. The pyroclastic density currents generally appear to have followed topography, indicating that they were low energy, high density pyroclastic density currents, consistent with their high emplacement temperatures.

[46] Paleomagnetic techniques offer a useful correlation tool for the ignimbrites of the APVC. Future studies can use this approach as a first choice for identifying ignimbrites of unknown provenance. Further work in Argentina and Bolivia may allow for the development of a more complete paleomagnetic database for the region. More data will allow for a better defined estimate of the ChRM directions for each ignimbrite, and the magnitude of dispersion may be related to cooling rate. Our paleomagnetic data were used by *Salisbury et al*. [2011] to help determine the provenance of ignimbrites in the APVC and develop estimates of eruptive volumes over time within the APVC.

Acknowledgments

[47] This work is part of a collaborative project funded by the National Science Foundation (EAR-0710545 and EAR-0538159). The enthusiastic support of Victor Ramirez, Paola Ballon Sanchez, Victor Quispe, and Lidia Nina during fieldwork is gratefully acknowledged. Timothy Murray, Caitlin Roeder, and, especially, Tyler Brown are thanked for their careful analytical work in the paleomagnetism laboratory at NAU. Miguel Garcés and Bet Beamud graciously provided complete access to the paleomagnetism laboratory at the Consejo Superior de Investigaciones Científicas' Institut de Ciències de la Terra "Jaume Almera" and Universitat de Barcelona during MHO's sabbatical there, and Elena Zanella and Roberto Lanza kindly hosted MHO at the Alpine Laboratory of Paleomagnetism in Peveragno, Italy. Extensive and constructive reviews by John Geissman and an anonymous reviewer greatly improved the manuscript. Morgan Salisbury is thanked for productive discussions.

References

Bachmann, O., C. F. Miller, and S. L. de Silva (2007), The volcanic–plutonic connection as a stage for understanding crustal magmatism, *J. Volcanol. Geotherm. Res.*, *167*, 1–23.

Baer, E. M., R. V. Fisher, M. Fuller, and G. Valentine (1997), Turbulent transport and deposition of the Ito pyroclastic flow: determinations using anisotropy of magnetic susceptibility, *J. Geophys. Res.*, *102*, 22565–22586.

Barke, R., S. Lamb, and C. MacNiocaill (2007), Late Cenozoic bending of the Bolivian Andes: New paleomagnetic and kinematic constraints, *J. Geophys. Res.*, *112*, B01101, doi:10.1029/2006JB004372.

Beck, M. E., Jr. (2004), The Central Andean rotation pattern: Another look, *Geophys. J. Int.*, *15*, 1348–1358.

Best, M. G., and E. H. Christiansen (1991), Limited extension during peak tertiary volcanism, Great-Basin of Nevada and Utah, *J. Geophys. Res.*, *96*, B13509–B13528.

Cas, R. A. F., H. M. N. Wright, C. B. Folkes, C. Lesti, M. Porreca, G. Giordano, and J. G. Viramonte (2011), The flow dynamics of an extremely large volume pyroclastic flow, the 2.08-Ma Cerro Galán Ignimbrite, NW Argentina, and comparison with other flow types, *Bull. Volcanol.*, *73*, 1583–1609.

Champion, D. E., and J. M. Donnelly-Nolan (1994), Duration of eruption of the Giant Crater lava field, Medicine Lake volcano, California, based on paleomagnetic secular variation, *J. Geophys. Res.*, *99*, B15595–B15604.

Coutand, I., A. Chauvin, P. R. Cobbold, and P. Gautier (1999), Vertical axis rotations across the Puna plateau (northwestern Argentina) from paleomagnetic analysis of Cretaceous and Cenozoic rocks, *J. Geophys. Res.*, *104*, 22965–22984.

de Silva, S. L., and P. W. Francis (1989), Correlation of large volume ignimbrites - two case studies from the central Andes of N. Chile, *J. Volcanol. Geotherm. Res.*, *37*, 133–149.

de Silva, S. L., and P. W. Francis (1991), Volcanoes of the Central Andes, Springer-Verlag, Heidelberg.

de Silva, S. L., and W. D. Gosnold (2007), Episodic construction of batholiths: Insights from the spatiotemporal development of an ignimbrite flare-up, *J. Volcanol. Geotherm. Res.*, *167*, 320–335.

de Silva, S., G. Zandt, R. Trumbull, and J. Viramonte (2006), Large-scale silicic volcanism – the result of thermal maturation of the crust, in Advances in Geosciences, edited by Y.-T. Chen and W.-H. Ip, pp. 215–230, World Scientific Press, Singapore.

Dekkers, M. J. (2009), Magnetic Proxy Parameters, in Encyclopedia of Geomagnetism and Paleomagnetism, edited by D. Gubbins and E. Herrero-Bervera, pp. 525–534, Springer, Dordrecht.

Elston, W. (1984), Mid-Tertiary ash flow tuff cauldrons, southwestern New Mexico, *J. Geophys. Res.*, *89*, B8733–B8750.

Fisher, R. V., G. Orsi, M. Ort, and G. Heiken (1993), Mobility of a large-volume pyroclastic flow - Emplacement of the Campanian Ignimbrite, Italy, *J. Volcanol. Geotherm. Res.*, *56*, 205–220.

Gardeweg, M., and C. F. Ramírez (1987), La Pacana caldera and the Atana ignimbrite—A major ash-flow and resurgent caldera complex in the Andes of northern Chile, *Bull. Volcanol.*, *49*(3), 547–566, doi:10.1007/BF01080449.

Geissman, J. W., D. Holm, S. S. Harlan, and G. F. Embree (2010), Rapid, high-temperature formation of large-scale

rheomorphic structures in the 2.06 Ma Huckleberry Ridge Tuff, Idaho, USA, *Geology*, *38*, 263–266, doi:10.1130/G30492.1.

Hagstrum, J. T., P. W. Lipman, and D. P. Elston (1982), Paleomagnetic evidence bearing on the structural development of the Latir volcanic field near Questa, New Mexico, *J. Geophys. Res.*, *87*, 7833–7842.

Hargraves, R. B., D. Johnson, C. Y. Chan (1991), Distribution anisotropy; the cause of AMS in igneous rocks?, *Geophys. Res. Lett.*, *18*, 2193–2196.

Hildreth, W. (1981), Gradients in silicic magma chambers: Implications for lithospheric magmatism, *J. Geophys. Res.*, *86*, B10153–B10192, doi:10.1029/JB086iB11p10153.

Hildreth, W., and G. Mahood (1985), Correlation of ashflow tuffs, *Geol. Soc. Am. Bull.*, *96*, 968–974, doi:10.1130/0016-7606(1985)96<968:COAT>2.0.CO;2.

Lamb, S. (2001), Vertical axis rotation in the Bolivian orocline, South America 1. Paleomagnetic analysis of Cretaceous and Cenozoic rocks, *J. Geophys. Res.*, *106*, 26605–26632.

Lindsay, J. M., A. K. Schmitt, R. B. Trumbull, S. L. de Silva, W. Siebel, and R. Emmermann (2001), Magmatic evolution of the La Pacana caldera system, central Andes, Chile: Compositional variation of two cogenetic, large-volume felsic ignimbrites, *J. Petrol.*, *42*, 459–486.

Lipman, P. W. (1984), The roots of ash flow calderas in western North America: Windows into the tops of granite batholiths, *J. Geophys. Res.*, *89*, B8801–B8841.

Lipman, P. W. (2007), Incremental assembly and prolonged consolidation of Cordilleran magma chambers: Evidence from the Southern Rocky Mountain volcanic field, *Geosphere*, *3*(1), 42–70, doi:10.1130/GES00061.1.

Lipman, P. W., M. A. Dungan, L. L. Brown, and A. Deino (1996), Recurrent eruption and subsidence at the Platoro caldera complex, southeastern San Juan volcanic field, Colorado: New tales from old tuffs, *Geol. Soc. Am. Bull.*, *108*, 1039–1055.

MacDonald, W. D., and H. C. Palmer (1990), Flow directions in ash-flow tuffs: a comparison of geological and magnetic susceptibility measurements, Tshirege member (upper Bandelier Tuff), Valles caldera, New Mexico, USA, *Bull. Volcanol.*, *53*, 45–59.

McIntosh, W. C. (1991), Evaluation of paleomagnetism as a correlation criterion for Mogollon-Datil Ignimbrites, Southwestern New Mexico, *J. Geophys. Res.*, *96*, 13459–13513.

Ort, M. H. (1993), Eruptive processes and caldera formation in a nested downsag-collapse caldera: Cerro Panizos, central Andes Mountains, *J. Volcanol. Geotherm. Res.*, *56*, 221–252.

Ort, M. H., M. Rosi, and C. D. Anderson (1999), Correlation of deposits and vent locations of the proximal Campanian Ignimbrite deposits, Campi Flegrei, Italy, based on NRM and AMS characteristics, *J. Volcanol. Geotherm. Res.*, *91*, 167–178.

Ort, M. H., G. Orsi, L. Pappalardo, and R. V. Fisher (2003), Anisotropy of magnetic susceptibility studies of depositional processes in the Campanian Ignimbrite, Italy, *Bull. Volcanol.*, *65*, 55–72.

Palmer, H. C., and W. D. MacDonald (1999), Anisotropy of magnetic susceptibility in relation to source vents of ignimbrites: empirical observations, *Tectonophysics*, *307*, 207–218.

Paquereau-Lebti, P., M. Fornari, P. Roperch, J. -C. Thouret, and O. Macedo (2007), Paleomagnetism, magnetic fabric, and $^{40}Ar/^{39}Ar$ dating of Pliocene and Quaternary ignimbrites in the Arequipa area, southern Peru, *Bull. Volcanol.*, *70*, 977–997, doi:10.1007/s00445-007-0181-y.

Petronis, M. S., and J. W. Geissman (2009), Anisotropy of magnetic susceptibility data bearing on the transport direction of mid-tertiary regional ignimbrites, Candelaria Hills area, west-central Nevada, *Bull. Volcanol.*, *71*, 121–151.

Pioli, L., R. Lanza, M. H. Ort, and M. Rosi (2008), Magnetic fabric, welding texture and strain fabric in the Nuraxi tuff, Sardinia, Italy, *Bull. Volcanol.*, *70*, 1123–1137.

Prezzi, C. B. (1999), Paleomagnetismo de rocas terciarias de la Puna jujeña (23° S, 66° 30′ O): ausencia de rotaciones según ejes verticals, *Rev. Asoc. Geol. Arg.*, *54*, 407–419.

Prezzi, C. B., and R. N. Alonso (2002), New paleomagnetic data from the northern Argentina Puna: Central Andes rotation pattern reanalyzed, *J. Geophys. Res.*, *107*, doi:10.1029/2001JB00225.

Pritchard, M., and M. Simons (2002), A satellite geodetic survey of large-scale deformation of volcanic centres in the central Andes, *Nature*, *418*, 167–170.

Richards, D. R., R. F. Butler, and T. Sempere (2004), Vertical-axis rotations determined from paleomagnetism of Mesozoic and Cenozoic strata of the Bolivian Andes, *J. Geophys. Res.*, *109*, B07104, doi:10.1029/2004JB002977.

Riehle, J. R. (1973), Calculated compaction profiles of rhyolitic ash-flow tuffs, *Geol. Soc. Am. Bull.*, *84*, 2193–2216.

Rochette, P., M. Jackson, and C. Aubourg (1992), Rock magnetism and the interpretation of the anisotropy of magnetic susceptibility, *Rev. Geophys.*, *30*, 209–226.

Roperch, P., M. Fornari, G. Hérail, and G. V. Parraguez (2000), Tectonic rotations within the Bolivian Altiplano: Implications for the geodynamic evolution of the central Andes during the late Tertiary, *J. Geophys. Res.*, *105*, 795–820.

Rousse, S., S. Gilder, M. Fornari, and T. Sempere (2005), Insight in the Neogene tectonic history of the northern Bolivian Orocline from new paleomagnetic and geochronologic data, *Tectonics*, *24*, TC6007, doi:10.1029/2004TC001760.

Salisbury, M. J., B. R. Jicha, S. L. de Silva, B. S. Singer, N. Jiménez-C., and M. H. Ort (2011), $^{40}Ar/^{39}Ar$ chronostratigraphy of Altiplano-Puna Volcanic Complex ignimbrites reveals the development of a major silicic magmatic province, *Geol. Soc. Am. Bull.*, *123*, 821–840, doi:10.1130/B30280.1.

Smith, R. L. (1979), Ash-flow magmatism, in Ash-Flow Tuffs, Geol. Soc. Amer. Spec. Pap., vol. *180*, edited by C. E. Chapin and W. E. Elston, pp. 5–27, Boulder, Colo.

Somoza, R., S. Singer, B. Coira, J. F. Vilas, A. Díaz, and P. Caffe (1994), Ignimbritas del complejo volcánico Vilama (22,6°S – 67°O). Correlaciones paleomagnéticas y petrológicas, 7° Congreso Geológico Chileno, *Actas*, *1*, 179–183.

Somoza, R., S. Singer, and B. Coira (1996), Paleomagnetism of upper Miocene ignimbrites at the Puna: An analysis of vertical-axis rotations in the Central Andes, *J. Geophys. Res.*, *101*, B11387–B11400.

Somoza, R., S. Singer, and A. Tomlinson (1999), Paleomagnetic study of upper Miocene rocks from northern Chile: Implications for the origin of late Miocene-Recent tectonic rotations in the southern Central Andes, *J. Geophys. Res.*, *104*, B22923–B22936.

Speranza F., A. Di Chiara, and S. G. Rotolo (2012), Correlation of welded ignimbrites on Pantelleria (Strait of Sicily) using paleomagnetism, *Bull. Volcanol.*, *74*, 341–357, doi:10.1007/s00445-011-0521-9.

Tauxe, L., C. Constable, C. L. Johnson, A. A. P. Koppers, W. R. Miller, and H. Staudigel (2003), Paleomagnetism of the southwestern U.S.A. recorded by 0–5 Ma igneous rocks, *Geochem. Geophys. Geosyst.*, *4*, 8802, doi:10.1029/2002GC000343.

Taylor, G. K., J. Grocott, B. Dashwood, M. Gipson, and C. Arévalo (2007), Implications for crustal rotation and tectonic evolution in the central Andes fore arc: New paleomagnetic results from the Copiapó region of northern Chile, 26°-28°S, *J. Geophys. Res.*, *112*, B01102, doi:10.1029/2005JB003950.

Vestine, E. H., L. Laporte, C. Cooper, I. Lange, and W. C. Hendrix (1959), Description of the Earth's main magnetic field and its secular change, 1905–1945, *Carnegie Inst. Washington Publ.*, *578*, 532.

Walker, J. D., and J. W. Geissman (2009), Commentary: 2009 GSA geologic time scale, *GSA Today*, *19*/4, 60–61.

Watts, R. B., S. L. de Silva, G. Jimenez, and I. W. Croudace (1999), Effusive silicic volcanism triggered and fueled by recharge: A case study of the Cerro Chascon–Runtu Jarita complex of SW Bolivia, *Bull. Volcanol.*, *61*, 241–264, doi:10.1007/s004450050274.

Wells, R. E., and J. W. Hillhouse (1989), Paleomagnetism and tectonic rotation of the lower Miocene Peach Springs Tuff: Colorado Plateau, Arizona, to Barstow, California, *Geol. Soc. Am. Bull.*, *101*, 846–863.

Zandt, G., M. Leidig, J. Chmielowski, D. Baumont, and X. H. Yuan (2003), Seismic detection and characterization of the Altiplano-Puna magma body, central Andes, *Pure Appl. Geophys.*, *160/3-4*, 789–807.

Zijderveld, J. D. A. (1967), AC demagnetization of rocks: analysis of results, in Methods in palaeomagnetism, edited by S.K. Runcorn, K. M. Creer and D. W. Collinson, pp. 254–286, Elsevier, Amsterdam.